AIAA JOURNAL
Vol. 43, No. 12, December 2005

Direct Simulation Monte Carlo Simulations of Hypersonic Flows with Shock Interactions

James N. Moss*
NASA Langley Research Center, Hampton, Virginia 23681-2199
and
Graeme A. Bird†
G.A.B. Consulting Pty. Ltd., Sydney, New South Wales 2000, Australia

The capabilities of a relatively new direct simulation Monte Carlo (DSMC) code are examined for the problem of hypersonic laminar shock/shock and shock/boundary-layer interactions, where boundary-layer separation is an important feature of the flow. Flow about two model configurations is considered, where both configurations (a biconic and a hollow cylinder-flare) have recent published experimental measurements. The computations are made using the DS2V code of Bird, a general two-dimensional/axisymmetric time-accurate code. The current focus is on flows produced in ground-based facilities at Mach 12 and 16 test conditions with nitrogen as the test gas and the test models at zero incidence. The freestream Knudsen numbers, with the characteristic length equal to the test model diameter, range from 0.0008 to 0.0004, consequently demanding computations for DSMC simulations. Results presented highlight the sensitivity of the calculations to grid resolution, sensitivity to physical modeling parameters, and comparison with experimental measurements. Information is provided concerning the flow structure and surface results for the extent of separation, heating, pressure, and skin friction.

Nomenclature

$a_{C,V}$ = surface accommodation for vibrational energy
C_f = friction coefficient, $\tau_w/(0.5\rho_\infty V_\infty^2)$
C_H = heat transfer coefficient, $q_w/(0.5\rho_\infty V_\infty^3)$
C_p = pressure coefficient, $(p_w - p_\infty)/(0.5\rho_\infty V_\infty^2)$
d = maximum double cone diameter, m
L = length of first cone projected on X axis, m
M_∞ = freestream Mach number
m = mass of a molecule, kg/m^3
mcs = mean collision separation distance, m
mfp = mean free path, m
mpc = molecules per cell
n = number density, m^{-3}
p = pressure, N/m^2
q = wall heat transfer rate, kW/m^2
R = reattachment location, m
Re_∞ = unit Reynolds number, $\rho_\infty V_\infty/\mu_\infty$, m^{-1}
S = separation location, m
T = temperature, K
u_n = velocity component normal to surface, m/s
u_p = velocity component parallel to surface, m/s
V_∞ = freestream velocity, m/s
x, y = model coordinates, m
ρ = density, kg/m^3
τ = viscous shear stress, N/m^2

Subscripts

R = rotational temperature or reattachment
S = separation
T = translational temperature
V = vibrational temperature
W = wall
∞ = freestream

Presented as Paper 2004-2585 at the AIAA 37th Thermophysics Conference, Portland, OR, 28 June–1 July 2004; received 29 July 2004; revision received 15 April 2005; accepted for publication 22 April 2005.

*Senior Research Engineer, MS 408A, Aerothermodynamics Branch; j.n.moss@larc.nasa.gov. Fellow AIAA.

†President, 144/110 Sussex Street; also Professor Emeritus, School of Aerospace, Mechanical and Mechatronic Engineering, University of Sydney, Sydney, New South Wales 2006, Australia; gabird@compuserve.com. Fellow AIAA.

Introduction

HYPERSONIC flow interactions between shocks and separated-flow regions produce very challenging problems for both experimental measurements and numerical simulations. An understanding of such interactions is critical to the design of hypersonic vehicles because these interactions can have a significant impact on both heating rates and vehicle aerodynamics, which in turn influence the requirements for vehicle control and thermal protection. Many experimental and theoretical studies dealing with shock/shock and shock/boundary-layer interactions over compression ramps were conducted in the last half century, and a recent review of some of the key findings for laminar flows is presented by Marini.[1] More recently, the NATO Research Technology Organization (RTO), under the coordination of Working Group 10,[2,3] has fostered a series of experimental and numerical studies focused on hypersonic flows. Two basic axisymmetric model configurations included in the RTO studies were a biconic and a hollow-cylinder flare. The current computational study focuses on the complex interactions resulting from hypersonic flows about these two configurations for experimental test conditions where separation and reattachment occur under laminar conditions.

This paper presents computational results obtained with the direct simulation Monte Carlo (DSMC) method[4–6] for two of a larger set of test cases that have been proposed for code validation studies. Both test cases are demanding for DSMC simulation because much of the flow domain is in the continuum regime; obvious exceptions are the flow near the sharp leading edges and along the surface, where velocity slip and temperature jump effects are significant. Furthermore, both the locations and physical properties of the shocks and their interaction regions are very sensitive to the cell/grid resolution used in a simulation. The flow conditions simulated are those for two experimental conditions performed by M. S. Holden and T. P. Wadhams (private communication, May 2003), one for Mach 15.6 nitrogen flow about a 25-/55-deg biconic model in the Calspan–University at Buffalo Research Center (CUBRC) 48-Inch Shock Tunnel and the

second from the measurements made for Mach 12.4 nitrogen flow about a hollow cylinder-flare (30-deg flare) model in the CUBRC Large Energy National Shock (LENS) Tunnel. Details concerning the experimental measurements are given in Refs. 7 and 8, and a listing of the flow conditions for the two test cases considered in the present study is included in Ref. 9.

Several DSMC studies have shown that the calculation of such problems under continuum conditions can be very demanding in terms of computer resources, both in time and in memory. In fact, results of the initial comparisons[10] of several DSMC calculations with measurements showed that the DSMC computations failed to predict the correct details of the separated region. Results of subsequent DSMC studies presented in Ref. 9 suggest that the failure to predict the details of the separation region was due primarily to inadequate grid resolution. A second finding from the initial comparisons of Harvey et al.[10] was that both DSMC and computational fluid dynamics (CFD) solutions differed substantially (as much as 33%, as discussed in Ref. 11) from the measured heating rates upstream of the separated region, that is, for laminar flow about both sharp[11] and blunted[12] cones at zero incidence. With differences of this magnitude, additional CFD studies[13] were conducted to reexamine the freestream flow conditions for which the CUBRC measurements were made. The findings of the Candler et al.[13] study for the CUBRC experiments showed that the freestream conditions had a significant level of thermal nonequilibrium (initially assumed to be in equilibrium) resulting from vibrational freezing during the nozzle expansion, confirming the earlier assessment of Roy et al.[12] The current calculations are made for one of the revised set of freestream conditions (hollow cylinder flare, run 11 conditions) and one for a biconic in a low-density condition (run 7).

Experimental evidence[14] suggests that when there is significant vibrational nonequilibrium within the shock layer, as is the case in the current problems, the vibrational energy does not accommodate to the surface temperature when the molecules impact the surface. Calculated results for both test cases show a reduction of approximately 12% in surface heating rate when the surface is assumed to have zero rather than full thermal accommodation for the vibrational energy. Also, the calculations show that the assumption concerning surface vibrational energy accommodation has no impact on surface pressure or the extent of separation. Comparisons with the CUBRC measurements for heating and pressure show generally good agreement, with differences in heating on the order of 15% or less, much less for these two test cases when full thermal accommodation is assumed.

DSMC Program

The DSMC program used in the current study is the DS2V program of Bird,[4–6] a general two-dimensional/axisymmetric code that provides both time-accurate unsteady flow and time-averaged steady flow simulations. Molecular collisions are simulated with the variable hard-sphere molecular model. Energy exchange between kinetic and internal modes is controlled by the Larsen–Borgnakke statistical model.[15] For the present study, the simulations are performed using nonreacting gas models while considering energy exchange between translational, rotational, and vibrational modes. The nitrogen molecular gas constants used in the current study are those given in Ref. 4. Also, a rotational relaxation collision number of 5 and a temperature-dependent vibrational collision number (Eq. 6.53 of Ref. 4) were used.

The DS2V program has the option of specifying multiple freestream temperatures, as is appropriate for the test cases currently investigated. The model surface is assumed to have a specified constant temperature, and diffuse reflection is assumed for the gas–surface interactions unless noted otherwise. Two options are exercised concerning surface thermal accommodation: one in which all energy modes are fully accommodated and one in which all energy modes, except for vibration, are fully accommodated ($a_{C,V} = 0$).

The DS2V program has taken advantage of several important developments[5,6] in DSMC methodology over the past decade, two of which will be briefly described. One is the use of transient subcells, in which a transient background grid is applied one cell at a time within the collision routine to promote nearest-neighbor collisions. The resolution of the transient background grid is a function of the number of molecules in the cell, that is, approximately one simulated molecule within each grid subcell. The ratio of the mean collision separation between collision partners to the local mean free path (mcs/mfp) should be less than one, and this parameter is currently being used as an indicator of the resolution achieved in a given simulation. One option for achieving a small value for this parameter is to increase the number of simulated molecules, which can be exercised any time during the simulation. Such an approach is demonstrated in the current study.

A second new feature of the current program is the manner in which the time step is established for uncoupling the molecular motion and collisions. Rather than use a single time step over the whole flow field or multiple subdomains, with each domain having a different time step, new procedures are used in which the time step varies with every molecule and every cell. These procedures, described in Refs. 5 and 6, keep all the time variables concurrent with the overall flow time. The overall flow time step is advanced in very small time increments (a fraction of the local mean collision time, which is kept for each cell). For an overall time step, only a small fraction of the molecules is moved, and only a small fraction of the molecules experiences collisions.

The flowfield cells are created from rectangular structures that consist initially of divisions, but from elements after the first grid adaption. After adaption, the cells are not necessarily rectangular because they are formed from one or more elements. The computational domain, which is initially divided into a Cartesian network of cells with a specified number of divisions in each of the coordinate directions, is bounded by user specified limits. If one is simulating a steady flow problem, the usual procedure is to advance the simulation until the flow achieves or approaches a steady state and then do a grid adaption. Adaption is achieved by creating new cells made up of one or more Cartesian elements (each division contains a fixed number of elements) so that each cell contains a specified number of simulated molecules. The transient subcells are set for each cell whenever collisions are to be calculated and are then discarded. The use of the transient subcells leads to nearest neighbor collisions.

Note that during a calculation interruption to either adapt the grid or change the number of simulated molecules, information at the time of interruption is retained, and the calculation continues to advance in time, with some time interval required before the perturbation effects, caused by an interruption, have been assimilated. The cell structure is set primarily by the DS2V program logic, and relatively little input is required of the user, which leads to a more user friendly program. Also, the new procedures are designed to be computationally fast, and the built-in flow visual displays provide instant access to the simulation parameters and results as they evolve with time.

Results and Discussion

Table 1 presents a summary of the freestream conditions for the two test cases investigated. The current paper presents results calculated with the DS2V program for the biconic at run 7 test conditions, as generated in the 48-Inch Shock Tunnel, and for the hollow cylinder-flare model at run 11 test conditions, as generated in the LENS I Tunnel. The Mach and Reynolds numbers listed are those provided for the respective test facilities and are based on the freestream translational temperatures. The freestream mean free path is approximately 0.219 and 0.084 mm for run 7 and 11 conditions, respectively.

Biconic Calculations for CUBRC Run 7 Test Conditions

The geometry and dimensions for the sharp 25 deg/55 deg double-cone model used in the current calculations are shown in Fig. 1. Reference 8 provides information regarding the experimental procedures and instrumentation that was used to obtain the heat transfer and pressure measurements that are compared with the present computations.

Table 2 presents a summary of some of the numerical parameters used in the calculations, along with results for the locations and

Table 1 Freestream and surface conditions for biconic and hollow cylinder-flare calculations

Run	V_∞, m/s	n_∞, m^{-3}	$T_{\infty,T}$, K	ρ_∞, kg/m^3	p_∞, N/m^2	M_∞	Re_∞, m^{-1}	Gas
48-Inch run 7	2073	3.779×10^{21}	42.6[a]	1.757×10^{-4}	2.23	15.6	1.37467×10^5	N_2
LENS run 11	2484	1.197×10^{22}	95.6[b]	5.566×10^{-4}	15.86	12.4	2.08333×10^5	N_2

[a]$T_{\infty,T} = T_{\infty,R} = 42.6$ K and $T_{\infty,V} = 1986$ K. [b]$T_{\infty,T} = T_{\infty,R} = 95.6$ K and $T_{\infty,V} = 2487$ K.

Table 2 DSMC numerical parameters[a] and results for sharp double cone (25, 55 deg): run 7 test conditions

Solution	△ time, ms	mpc	Molecules	mcs/mfp	Vib. accom.	x_S, mm	x_R, mm	Δx, mm
a0	1.27 to 1.91	10	0.514E+6	0.944	0.0	82.8	99.4	16.6
b0	3.30 to 3.65	10	1.980E+6	0.441	0.0	81.2	100.4	19.2
c0	3.84 to 3.97	40	8.136E+6	0.214	0.0	80.3	100.7	20.4
d0	3.97 to 4.41	40	8.114E+6	0.213	0.0	80.4	100.8	20.4
a1	1.03 to 2.02	10	0.528E+6	0.946	1.0	82.6	99.6	17.0
b1	3.30 to 3.65	10	1.980E+6	0.441	1.0	81.1	100.4	19.3
c1	3.83 to 3.96	40	8.133E+6	0.214	1.0	80.4	100.8	20.4
d1	3.96 to 4.40	40	8.114E+6	0.213	1.0	80.4	100.8	20.4
e1	4.81 to 4.93	40	16.482E+6	0.147	1.0	80.1	101.0	20.9

[a]Divisions = 151 × 181, elements per division = 20 × 20, and radial weighting factor = 100.

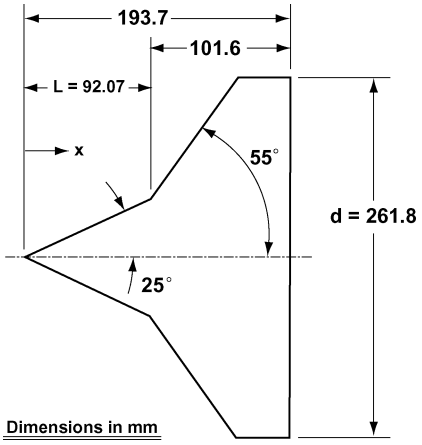

Fig. 1 CUBRC sharp double-cone model, where x is measured from the vertex.

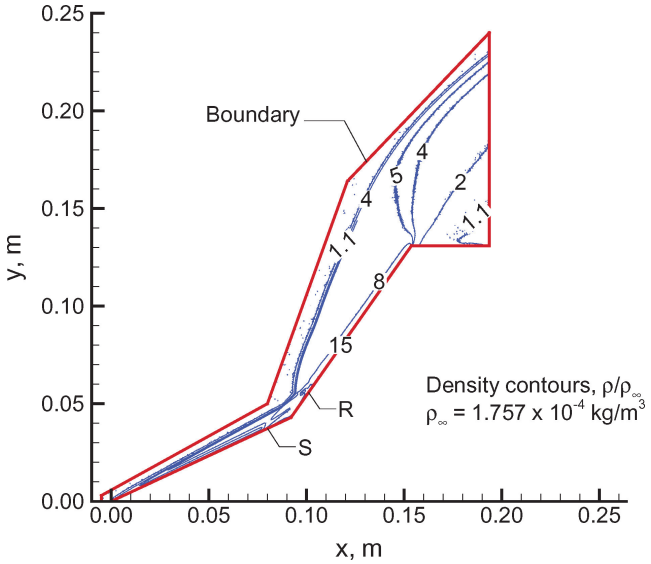

Fig. 2 Density contours from solution e1 for CUBRC run 7 conditions.

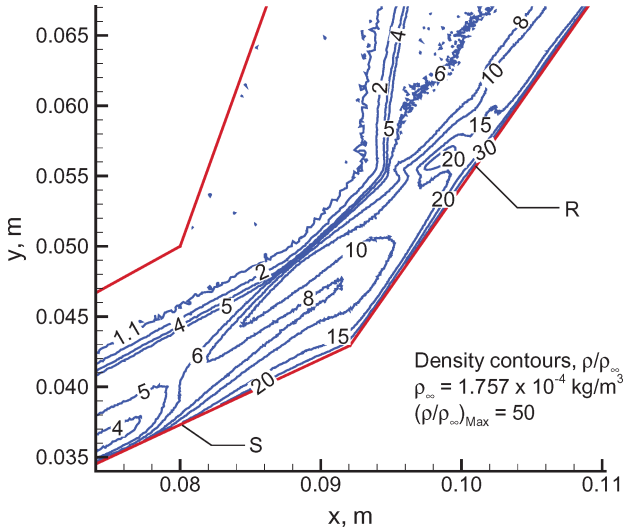

Fig. 3 Density contours in separation region for run 7 conditions, solution e1.

the extent of the separation region. Surface sampling cells were specified as follows: 100 along the forecone, 150 along the second cone, and 15 along the model extension. Figures 2–15 present details concerning the calculated flow structure and surface results. Two separate series of calculations are made where the surface thermal accommodation for the vibrational energy is the only variable, zero accommodation for the lettered solutions with a "0" extension, and full accommodation for the lettered solutions with a "1" extension, as listed in Table 2. Results for these time-accurate solutions are included for flow times of approximately 1 to 5 ms.

Figures 2–6 present flowfield contours that describe many of the flow features for the current problem and the computational domain (Fig. 2) used to perform the numerical simulations. Figure 7 presents contours for the ratio of the mean collision separation distance to the mean free path (mcs/mfp), a parameter used to measure the quality of the simulation where it is desirable that the parameter be less than one throughout the computational domain. Furthermore, Figs. 8–15 provide calculated surface distributions for velocity slip, temperature jump, heating, pressure, and friction, along with some insight into how these quantities are influenced by computational resolution, how the calculated data compare with the CUBRC surface heating and pressure measurements, and how the current computations compare with those from another DSMC program called SMILE[16] (statistical modeling in low-density environment).

Closer examination of the data presented in Figs. 2–15 reveals several points of interest. First, the application of the DS2V code provides results that are in good (less than 10%) to fair (10–15%

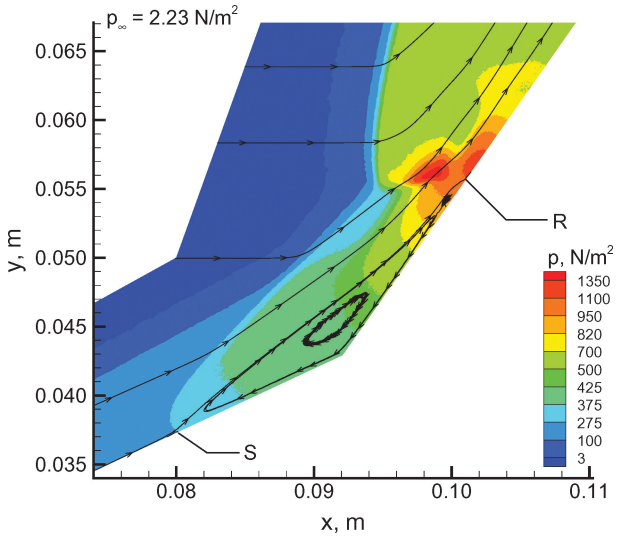

Fig. 4 Pressure contours and streamlines in separation region for run 7 conditions, solution e1.

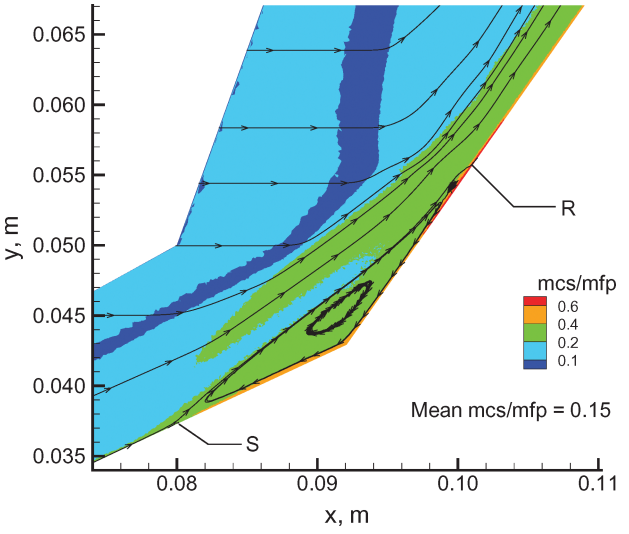

Fig. 7 Ratio of mean collision separation to mean free path (mcs/mfp) contours and streamlines in separation region for run 7 conditions, solution e1.

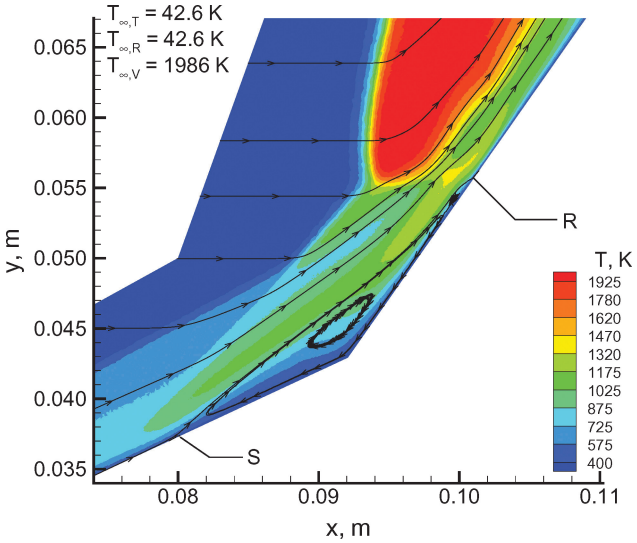

Fig. 5 Overall kinetic temperature contours and streamlines in separation region for run 7 conditions, solution e1.

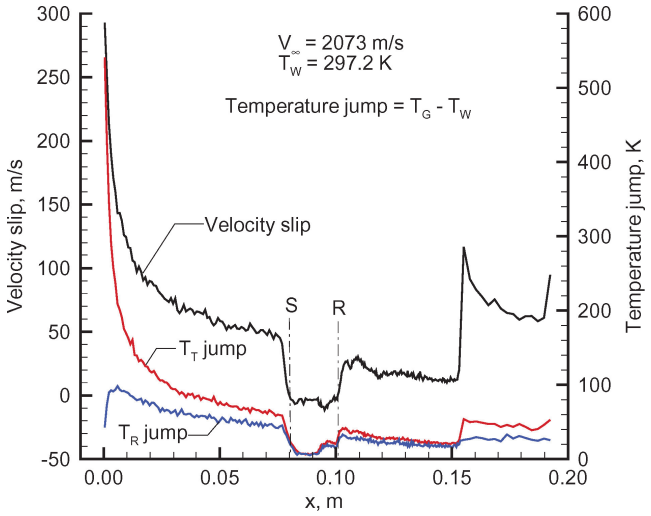

Fig. 8 Calculated surface distributions for velocity slip and temperature jump, both translational and rotational, for run 7 conditions, solution e1.

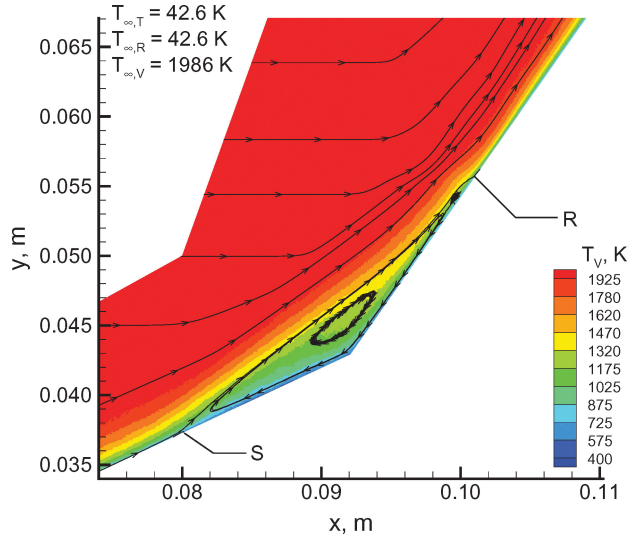

Fig. 6 Vibrational temperature contours and streamlines in separation region for run 7 conditions, solution e1.

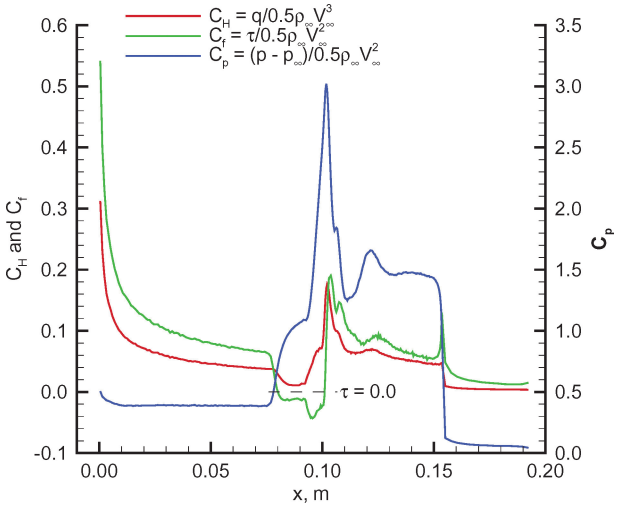

Fig. 9 Calculated surface distributions for heating, pressure, and friction for run 7 conditions, solution e1.

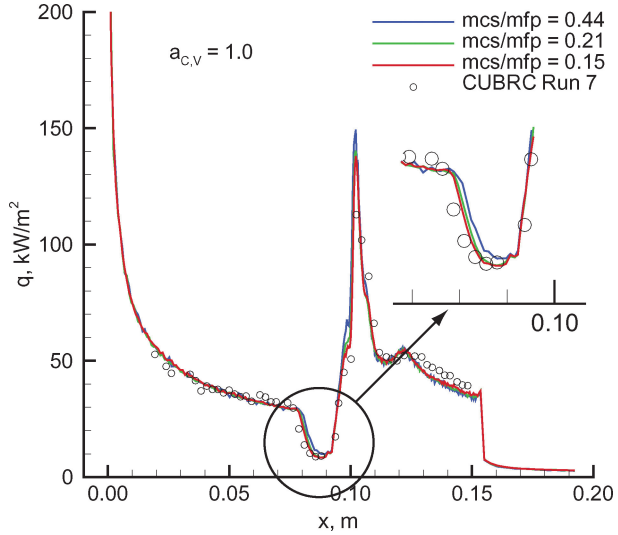

Fig. 10 Calculated and measured heating rates for run 7 conditions: effect of computational resolution.

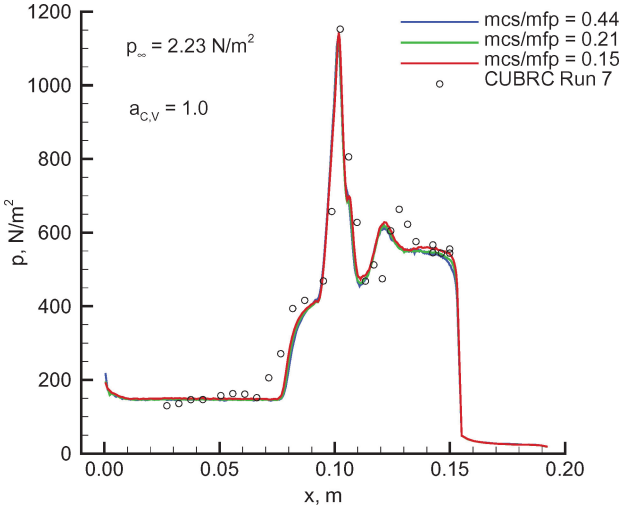

Fig. 11 Calculated and measured surface pressures for run 7 conditions: effect of computational resolution.

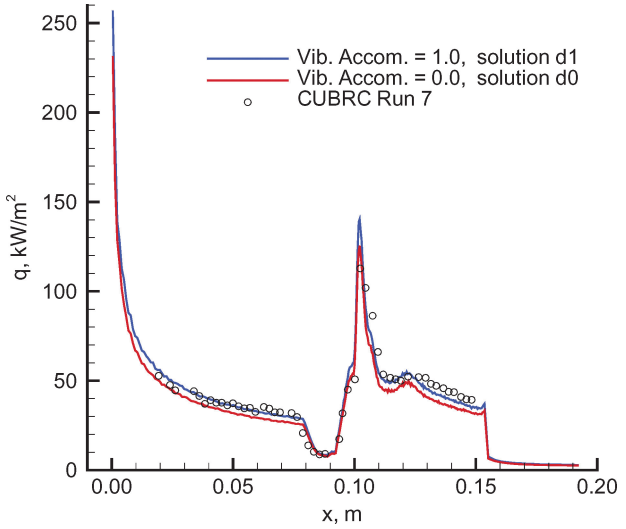

Fig. 12 Calculated and measured heating rates for run 7 conditions: effect of vibrational surface accommodation.

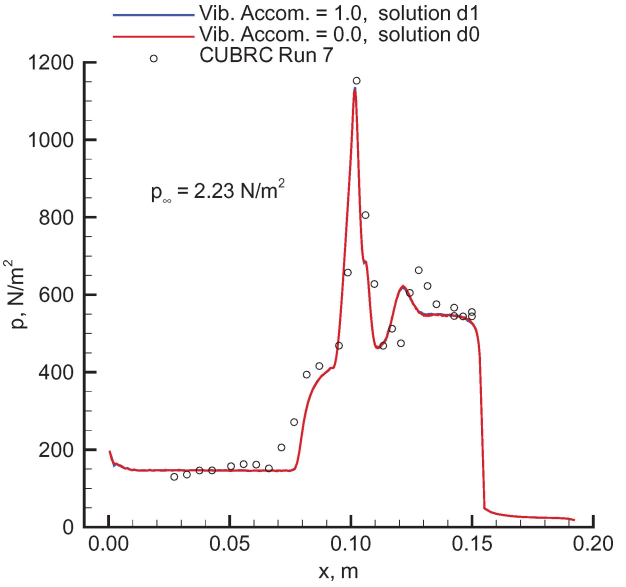

Fig. 13 Calculated and measured surface pressures for run 7 conditions: effect of vibrational surface accommodation.

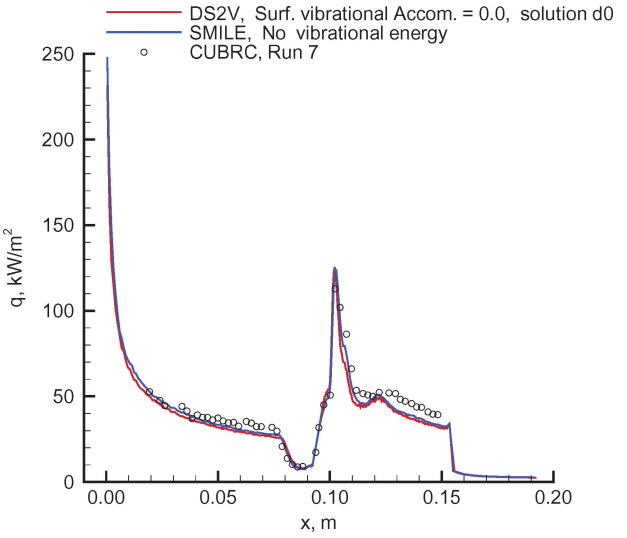

Fig. 14 Calculated and measured heating rates for run 7 conditions: results from two DSMC codes.

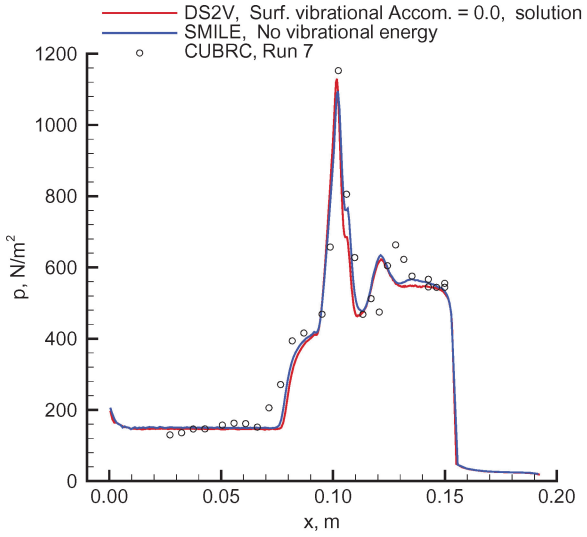

Fig. 15 Calculated and measured surface pressures for run 7 conditions: results from two DSMC codes.

difference) overall agreement (Figs. 10–15) with the experimental data. Second, the thermal nonequilibrium freestream condition persists within the shock layer (compare Figs. 5 and 6). Only within the boundary layer and near the surface is there evidence (Fig. 6) of significant depletion or equilibration of the vibrational energy, and only for the solution with full thermal accommodation at the surface. When the calculation is performed with no surface accommodation of the vibrational energy (solution d0), the vibrational temperature remains above 1925 K throughout the flowfield, essentially frozen at the elevated freestream condition. Calculations performed with the same freestream conditions, except that the vibrational temperature was set to that of the other temperature modes (42.6 K), resulted in lower heating rates (not shown) but showed no perceptible differences for surface pressure or friction. Third, the current time-accurate simulation suggests that this laminar flow test case, with boundary layer separation, stabilizes rather quickly, on the order of a millisecond. The longer run time used in the present study occurred because several numerical perturbations (grid adaption or increase in the number of simulated molecules) were imposed as the simulation evolved in time. The simulations were monitored to ensure that a steady state was achieved, followed by the generation of a significant time-averaged sample for the results listed in Table 2. The steady state aspect of the simulations is demonstrated in Table 2 for the c0/1 and d0/1 solutions, both with and without surface vibrational accommodation, where sequential time-averaged solutions yield essentially the same results for the separation region. Fourth, the current simulation approach has used computational cells that are coarse in relation to the local mean free path, but the simulation has used the transient subcell feature of the DS2V code, along with a large number of simulated molecules per cell, to promote small values of the local mcs/mfp parameter. For the most-resolved simulation, solution e1, the mean value of mcs/mfp was 0.15, with local values less than 0.37 at the location of separation and with no value exceeding 0.72.

Additional numerical studies would be useful in establishing bounds on the computational merit parameter mcs/mfp to ensure good engineering results for general applications. Obviously, if the parameter is sufficiently small, the results should be accurate but potentially demanding computationally. Also, a small mean value of the merit parameter is at best only a necessary condition for a good simulation, but not a sufficient condition, because of potentially large gradients, whereas local values of the merit parameter can be much larger than the mean value.

The biconic test cases produce large flowfield gradients due to shock interactions and substantial amplifications of surface loads caused by shock/boundary layer interactions, as is clearly evident for the CUBRC run 7 test case. Densities that equal 30 times the freestream value are evident within the shock layer (Fig. 3), and even higher densities (50 times free stream) occur along the second cone surface. The peak pressure amplification occurs off the surface (Fig. 4) with a magnitude that equals 670 times the freestream value, while the maximum overall kinetic temperature (Fig. 5) is 2050 K.

In Fig. 8, the calculated surface distributions for velocity slip and temperature jump, both translational and rotational, are presented. The maximum values for these quantities occur at or near the cone apex, then decrease with increasing distance downstream, decrease significantly in the separation region with a reversal in the sign of the slip velocity, and increase with the flow expansion at the aft end of the second cone.

The slip velocity V_s at a surface element may be determined from the incident and reflected velocities of the molecules that strike the element. If m is the mass of a molecule, u_p is the velocity component parallel to the surface, and u_n is the velocity component normal to the surface:

$$V_s = \frac{\sum(mu_p/|u_n|)}{\sum(m/|u_n|)} \tag{1}$$

Note that the sums are taken over both the incident and the reflected molecules. The expression for the slip velocity given by Eq. (1) differs from the standard definition of velocity in a spatial or volumetric element by the addition of the terms containing the normal velocity component. These additional terms transform the fluxal quantities in the surface samples to the spatial quantities in the gas immediately above the surface. Similar transformations have been made of the spatial definitions of translational and rotational temperature to determine the temperature jumps.

The slip velocity in a simulation is affected by the DSMC computational merit parameter mcs/mfp (if the merit parameter is too large, so is the slip velocity), as well as by physical factors such as the gas–surface interaction through the inclusion of a fraction of specular reflection at the surface. Additional details of the surface slip sensitivity to these parameters are given in Ref. 17, where it is shown that the size of the separation zone is directly related to the slip velocity, as affected by the quality of the computation. Also, it was demostrated that the direct manipulation of slip by surface motion (an incidental feature of the current program) had the same effect on the extent of separation as the quality of the simulation. Yet the alteration of the slip velocity by the gas–surface interaction had a very different effect; hence, the slip velocity cannot, by itself, be used to predict or correlate the extent of separation. Depending on factors that may or may not be accounted for in a given slip model (imposed boundary conditions for Navier–Stokes equations), very different flows may be associated with a given level of velocity slip, hence an obvious shortcoming of continuum models.

The calculated surface distributions for heating rate, pressure, and friction are presented in Figs. 9–15, in which Fig. 9 presents a summary of heating, pressure, and friction results (in coefficient form) for the most resolved calculation (solution e1), 16.5 million simulated molecules with a mean mcs/mfp value equal to 0.147. The maximum local values for the mcs/mfp parameter never exceeded 0.72, which occurred along the second cone. Figures 10 and 11 show the effect of reducing the mean value of mcs/mfp [first by a factor of 2 (increasing the number of molecules by a factor of 4) and then by a factor of 1.41] on heating and pressure distributions, respectively. The results included in Table 2 indicate the corresponding effect of reducing the magnitude of the mcs/mfp parameter from about 0.95 to 0.15 on the locations and extent of separation, with the extent of separation increasing with increased resolution. As shown in Figs. 10 and 11, the agreement between the finest resolution simulation (with $a_{C,V} = 1.0$) and the measurements is reasonably good, with the calculation predicting a slightly delayed separation relative to the experimental value.

The impact of the surface boundary condition for the vibrational energy accommodation is clearly evident on the surface heating, as is demonstrated in Fig. 12, where the heating rate is reduced by approximately 12% for zero accommodation, as compared to full accommodation. The impact of the vibrational energy accommodation boundary condition on surface pressure (Fig. 13) and the locations and extent of separation (Table 2) is negligible. The comparisons shown in Figs. 12 and 13 are made for the same grid resolution, solutions d1 and d0. The calculated heating rates are in better agreement with the CUBRC measurements for the assumption of full thermal accommodation and the same is shown later for the run 11 test case; therefore, one might be inclined to say that the full accommodation of the vibrational energy mode is more appropriate. However, results from additional calculations for only the forecone of the biconic model at other CUBRC test conditions (runs 28 and 35, as discussed in Ref. 18) show a different trend where the zero accommodation calculation for the vibrational energy mode provides better agreement with measurements. Therefore, it appears that the variability in the measured heating rate data, with respect to the DS2V calculations, is such that one is not able to resolve a 12% effect in heating; that is, to determine whether either of the vibrational accommodation boundary conditions is appropriate.

The final comparison for the run 7 calculations are the current DS2V results with those Markelov obtained by using the SMILE DSMC code, the same results that were included in a recent review paper by Harvey.[9] The SMILE calculations were made without accounting for the vibrational energy (vibration turned off), which should be very similar to the DS2V results with vibration included and zero accommodation for the vibrational energy at the surface.

Thus, the SMILE results are compared with data from solution d0. The two calculations for surface heating and pressure distributions are in very close agreement, as shown in Figs. 14 and 15, with the SMILE results, showing slightly better agreement with the experimental measurements, particularly for the extent of separation ($x_S = 79.6$ mm, $x_R = 101.1$ mm, and $\Delta x = 21.5$ mm). In the SMILE calculation, a parallel code implementation with 80 million simulated molecules was used, approximately an order of magnitude greater than that used in the single-processor DS2V calculation, solution d0.

Hollow Cylinder-Flare Calculations for CUBRC Run 11 Test Conditions

The CUBRC run 11 test case for the hollow cylinder-flare model was included in the present study because it has been investigated extensively with both CFD and DSMC methods for the initially reported[10] test conditions, has a small but distinct separation region, and has been examined recently with DSMC computations[9,19] as the freestream conditions were redefined[7] to account for vibrational nonequilibrium effects. Figure 16 presents details of the model configuration used in the present calculations. The hollow cylinder has a sharp leading edge with a bevel angle of 10 deg and is aligned parallel to the oncoming flow. The compression flare is inclined 30 deg to the cylinder. Surface sampling cells were specified as follows: 600 along the flare, 250 along the top surface of the cylinder, and 20 along the bevel leading edge.

An abbreviated presentation of the calculated results for the run 11 test case is given in Table 3 and Figs. 17–19, highlighting the comparison with the experimental measurements for surface heating and pressure. Figure 17 shows the computational boundary used in the present calculations, which includes a portion of the beveled leading edge. Also shown in Fig. 17 are selected density contours normalized by the freestream value, where the maximum value is 26.

Similarly to the run 7 solutions, two separate sets of calculations were made for run 11 conditions where the only variable was the surface accommodation for the vibrational energy. As listed in Table 3, the set of solutions with zero surface accommodation for the vibrational energy is denoted by a letter followed by "0," and the solutions with full accommodation are denoted by a letter followed by "1." For each set of calculations, some of the numerical parameters and results for the locations and extent of separation are included in Table 3, as the solutions were advanced in time with various perturbations accounting for grid adaption and increases in the number of simulated molecules. The steady-state aspect of the simulations is demonstrated in Table 3 for the g0/1 and h0/1 solutions, both with and without surface vibrational accommodation, where sequential time-averaged results provide essentially the same results for the

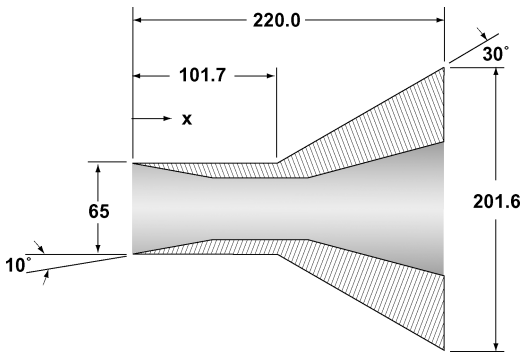

Fig. 16 CUBRC hollow cylinder-flare model (dimensions in millimeters), where x is measured from leading edge.

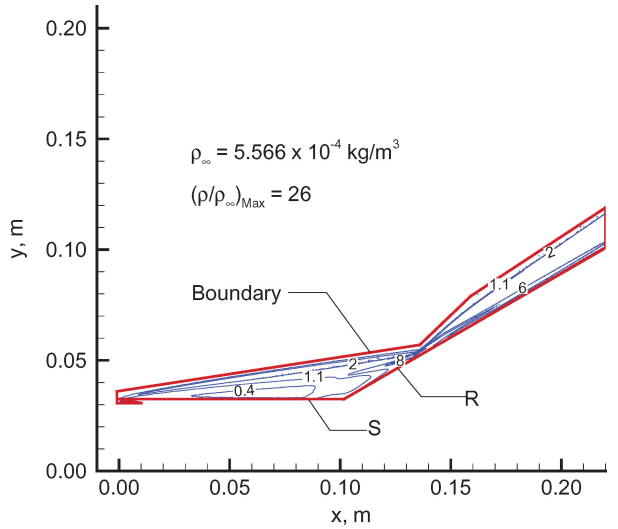

Fig. 17 Computational domain and density contours for run 11 conditions, solution j1.

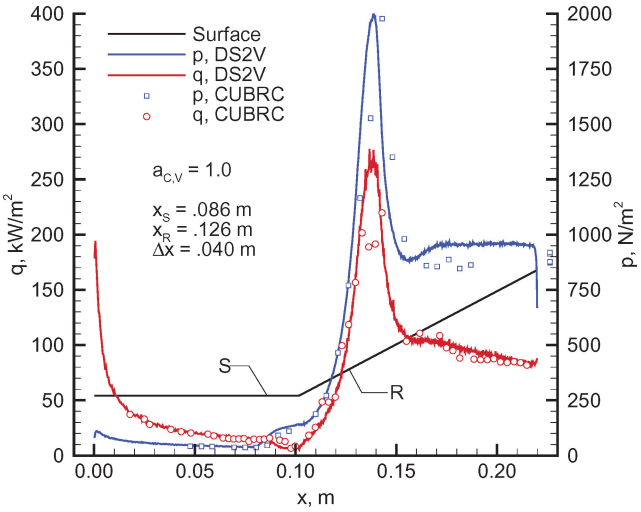

Fig. 18 Calculated and measured surface heating rate and pressure distributions for run 11 conditions, solution j1.

Table 3 DSMC numerical parameters[a] and results for a hollow cylinder-flare, run 11 test conditions

Solution	△ time, ms	mpc	Molecules	mcs/mfp	Vib. accom.	x_S, mm	x_R, mm	Δx, mm
f0	0.92 to 1.02	10	$1.707E+6$	0.781	0.0	93.6	122.1	28.5
g0	1.24 to 1.57	10	$1.705E+6$	0.782	0.0	91.1	122.8	31.7
h0	3.64 to 4.29	10	$1.639E+6$	0.768	0.0	90.8	122.5	31.7
i0	4.49 to 4.79	31	$5.200E+6$	0.440	0.0	88.8	124.9	36.1
j0	4.91 to 5.11	40	$10.339E+6$	0.306	0.0	86.1	126.3	40.2
f1	0.90 to 1.01	10	$1.682E+6$	0.775	1.0	94.2	121.2	27.0
g1	1.14 to 1.92	10	$1.706E+6$	0.785	1.0	90.8	122.2	31.4
h1	3.02 to 3.67	10	$1.641E+6$	0.770	1.0	90.4	122.7	32.3
i1	3.90 to 4.12	31	$5.106E+6$	0.436	1.0	88.6	124.9	36.3
j1	4.71 to 4.85	40	$10.337E+6$	0.307	1.0	86.2	126.3	40.1

[a]Divisions = 223 × 91, elements per division = 20 × 20, and no radial weighting factor.

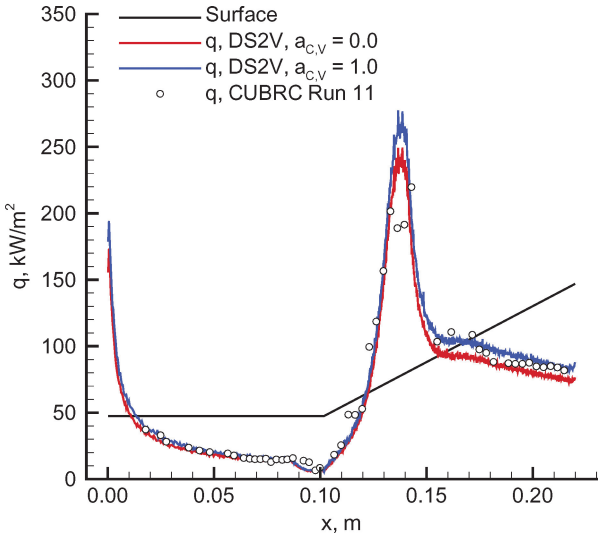

Fig. 19 Calculated effect of vibrational energy surface thermal accommodation on heating rate distribution for run 11 conditions, solutions j0 and j1.

locations and extent of the separation region. The best spatially resolved solutions (j0 and j1) had global mean values for mcs/mfp of 0.31 and maximum values of 0.25 and 0.75 at separation and reattachment, respectively. The maximum value of mcs/mfp was 1.2, and this value occurred along the surface in the region downstream of reattachment where the shock interactions produce a very thin shock layer.

Results calculated for the surface heating rate and pressure distributions, along with the location and extent of separation, are included in Fig. 18. Agreement between the calculated and the measured results are generally good for both the heating rate and pressure distributions (solution j1, Table 3), particularly the heating rate. For this test case, the calculated location of separation is slightly upstream of the results inferred from the heating and pressure measurements. Also evident in Fig. 18 are the rarefaction effects at the hollow cylinder leading edge, where both the heating rate and pressure increase as the leading edge is approached, reach their respective maximum and then decrease toward their free molecular values, failing to achieve the free molecular values because of upstream influence from the leading edge. Along the cylinder, the velocity slip and temperature jump are substantially larger than those experienced by the biconic model for run 7 conditions (Fig. 8), with leading edge values of approximately 875 m/s for the velocity slip and 1400 K for the translational temperature jump.

The calculated effect of surface thermal accommodation is addressed in the results presented in Fig. 19. The heating rate distribution, assuming full thermal accommodation (blue curve, solution j1 in Table 3), is about 12% higher than that obtained for the assumption that the surface vibrational energy is not accommodated (red curve, solution j0 in Table 3). As discussed in Ref. 15, there are experimental results for vibrationally nonequilibrium flows which suggest that the surface vibrational energy accommodation is very small and that a zero accommodation should be a realistic boundary condition for the present problems. Assuming full accommodation, the current calculations provide good agreement with the heating measurements but only fair agreement with the assumption of zero accommodation for the vibrational energy at the surface. As was the case for the run 7 calculations, the effect of the surface boundary condition on the separation region and the pressure distribution was negligible.

Conclusions

Results of a computational study are presented for hypersonic flows about biconic and hollow cylinder-flare models at zero incidence. The freestream conditions are those given for experiments conducted by CUBRC at Mach 15.6 and 12.4 in nitrogen in two shock tunnels, the 48-Inch Tunnel and the LENS I Tunnel, respectively. Computations are made with the DSMC method by using a relatively new and evolving time-accurate program under development by Bird (the second author), called DS2V. The focus of the current study is to examine the effectiveness of the DS2V code in predicting complex flows that result from shock/shock and shock/boundary layer interactions and problems where the calculated results are extremely sensitive to the numerical parameters used in the simulation. The overall comparisons of the present computations with both experimental and other computational results are shown to be good.

The results obtained for the CUBRC run 7 test case (biconic model) suggest the following: The current time-accurate calculations, made with a coarse cell structure but with a large number of molecules per cell (fairly small values of the mean collision separation to mean free path ratio (mcs/mfp)), give generally good agreement with the CUBRC data for surface heating and pressure. In particular, the heating rate comparisons show good agreement for the most refined calculations, with the assumption of full surface accommodation for the vibrational energy, but only fair agreement for the assumption of no surface accommodation of the vibrational energy, which produces a 12% reduction in the heating relative to the full accommodation assumption. Comparison of the present DS2V results with those obtained with the SMILE DSMC program shows very good agreement. Also, the thermal nonequilibrium freestream condition, with a highly elevated freestream vibrational temperature, persists throughout the shock layer for the assumption of zero surface accommodation of the vibrational energy. When a full thermal accommodation surface boundary condition is imposed, the vibrational energy within the shock layer experiences a significant depletion or adjustment adjacent to the surface, producing approximately a 12% increase in the surface heating rates.

For the CUBRC run 11 test case (hollow cylinder-flare model), the computed and measured surface results for heating rate and pressure showed the same general trends evident for the run 7 case; good agreement for heating rates with full surface accommodation but only fair agreement with zero surface accommodation for the vibrational energy (also, a 12% reduction in surface heating rates).

Even though the present comparisons of measured and calculated heating rates suggest that the full surface accommodation is the appropriate boundary condition, other calculations[18] that used the same DS2V program for higher density conditions but only along the forecone of the biconic model show the opposite trend; that is, the use of the zero accommodation for the vibrational energy provides better agreement with the CUBRC measurements. Consequently, the variability evident in the heating rate measurements, when compared to the DS2V calculations (of the order of $\pm 15\%$, Ref. 19) are such that it is difficult to isolate a 12% effect on heating rates, that is, what boundary condition is appropriate for the surface accommodation of the vibrational energy.

Acknowledgments

The authors acknowledge the assistance of Michael Holden and Timothy Wadhams of CUBRC for providing information regarding the model configurations, test flow conditions, and experimental results. Appreciation is also expressed to Gennady Markelov of Advanced Operations and Engineering Services, The Netherlands, for providing the computational results with the SMILE DSMC program.

References

[1]Marini, M., "Analysis of Hypersonic Compression Ramp Laminar Flows Under Sharp Leading Edge Conditions," *Aerospace Sciences and Technology*, Vol. 5, No. 4, 2001, pp. 257–271.

[2]Knight, D., "RTO WG 10: Test Cases for CFD Validation of Hypersonic Flight," AIAA Paper 2002-0433, Jan. 2002.

[3]Walker, S., and Schmisseur, J. D., "CFD Validation of Shock–Shock Interaction Flow Fields," AIAA Paper 2002-0436, Jan. 2002.

[4]Bird, G. A., *Molecular Gas Dynamics and the Direct Simulation of Gas Flows*, Clarendon, Oxford, 1994.

[5]Bird, G. A., *Visual DSMC Program for Two-Dimensional and Axially Symmetric Flows, The DS2V Program User's Guide*, Ver. 2.1, URL: http://gab.com.au [cited Nov. 2003].

[6]Bird, G. A., "The DS2V/3V Program Suite for DSMC Calculations," *Rarefied Gas Dynamics, 24th International Symposium*, Vol. 762, edited by M. Capitelli, American Inst. of Physics, Melville, NY, 2005, pp. 541–546.

[7]Holden, M. S., and Wadhams, T. P., "Code Validation Study of Laminar Shock/Boundary Layer and Shock/Shock Interactions in Hypersonic Flow. Part A: Experimental Measurements," AIAA Paper 2001-1031, Jan. 2001.

[8]Holden, M. S., Wadhams, T. P., Candler, G. V., and Harvey, J. K., "Measurements in Regions of Low Density Laminar Shock Wave/Boundary Layer Interaction in Hypervelocity Flows and Comparison with Navier–Stokes Predictions," AIAA Paper 2003-1131, Jan. 2003.

[9]Harvey, J. K., "A Review of a Validation Exercise on the Use of the DSMC Method to Compute Viscous/Inviscid Interactions in Hypersonic Flow," AIAA Paper 2003-3643, June 2003.

[10]Harvey, J. K., Holden, M. S., and Wadhams, T. P., "Code Validation Study of Laminar Shock/Boundary Layer and Shock/Shock Interactions in Hypersonic Flow. Part B: Experimental Measurements," AIAA Paper 2001-1031, Jan. 2001.

[11]Moss, J. N., "Hypersonic Flows About a 25° Sharp Cone," NASA TM-2001-211253, Dec. 2001.

[12]Roy, C. J., Bartel, T. J., Gallis, M. A., and Payne, J. L., "DSMC and Navier–Stokes Predications for Hypersonic Laminar Interacting Flows," AIAA Paper 2001-1030, Jan. 2001.

[13]Candler, G. V., Druguet, M.-C., Holden, M. S., Wadhams, T. P., Boyd, I. D., and Wang, W.-L., "CFD Validation for Hypersonic Flight: Hypersonic Double-Cone Flow Simulations," AIAA Paper 2002-0581, Jan. 2002.

[14]Meloans, J. G., and Graur, I., "New Thermal Conditions at the Wall in High Speed Flows," *Rarefied Gas Dynamics, 23rd International Symposium* [CD-ROM], Vol. 663, edited by A. D. Ketsdever and E. P. Muntz, American Inst. of Physics, Melville, NY, 2003.

[15]Borgnakke, C., and Larsen, P. S., "Statistical Collision Model for Monte Carlo Simulation of Polyatomic Gas Mixture," *Journal of Computational Physics*, Vol. 18, No. 4, 1975, pp. 405–420.

[16]Ivanov, M. S., Markelov, G. N., and Gimelshein, S. F., "Statistical Simulation of Reactive Rarefied Flows: Numerical Approach and Applications," AIAA Paper 98-2669, June 1998.

[17]Moss, J. N., and Bird, G. A., "DSMC Simulations of Hypersonic Flows with Shock Interactions and Validation with Experiments," AIAA Paper 2004-2585, June–July 2004.

[18]Moss, J. N., Bird, G. A., and Markelov, G. N., "DSMC Simulations of Hypersonic Flows and Comparison with Experiments," *Rarefied Gas Dynamics, 24th International Symposium*, Vol. 762, edited by M. Capitelli, American Inst. of Physics, Melville, NY, 2005, pp. 547–552.

[19]Markelov, G. N., Ivanov, M. S., Gimelshein, S. F., and Levin, D. A., "Statistical Simulation of Near-Continuum Flows With Separation," *Rarefied Gas Dynamics, 23rd International Symposium*, Vol. 663, edited by A. D. Ketsdever and E. P. Muntz, American Inst. of Physics, Melville, NY, 2003, pp. 457–464.

C. Kaplan
Associate Editor